doi: 10.1093/pasj/psx159

The Nature of EU Peg: an Algol-type Binary with a δ Scuti-type Component

Yuangui Yang[1], **Huiyu, Yuan**[1*], **Haifeng Dai**[1], **Xiliang Zhang**[2]

[1]Information College/School of Physics and Electronic Information, Huaibei Normal University, Huaibei 235000, Anhui Province, China

[2]Yunnan Observatories, Chinese Academy of Sciences, 396 Yangfangwang, Guandu District, Kunming 650216 China

*E-mail: yuanhy@chnu.edu.cn (Huiyu Yuan; corresponding author); yygcn@163.com

Received June 23, 2017; Accepted Dec 22, 2017

Abstract

The comprehensive photometry and spectroscopy for the neglected eclipsing binary EU Peg are presented. We determine its spectral type to be A3V. With the W-D program, the photometric solution was deduced from the four-color light curves. The results imply that EU Peg is a detached binary with a mass ratio of $q = 0.3105(\pm 0.0011)$, whose components nearly fills theirs Roche lobes. The low-amplitude pulsation occurs around the secondary eclipse, which may be attributed to the more massive component. Three frequencies are preliminarily explored by the Fourier analysis. The pulsating frequency at $f_1 = 34.1$ c/d is a *p*-mode pulsation. The orbital period may be undergoing a secular decrease, superimposed by a cyclic variation. The period decreases at a rate of $dP/dt = -7.34 \pm 1.06$ d yr^{-1}, which may be attributed to mass loss from system due to stellar wind. The cyclic oscillation, with $P_{mod} = 31.0 \pm 1.4$ yr and $A = 0.0054 \pm 0.0010$ day, may be interpreted by the light-time effect due to the assumed third body. With its evolution, the pulsating binary EU Peg will evolve from the detached configuration to semi-detached case.

Key words: stars: binaries: eclipsing; star: variables: delta Scuti; stars: individuals (EU Peg)

1 Introduction

Pulsations in eclipsing binaries are of particular interest for the theories of stellar formation, structure and evolution because binarity may provide accurate physical parameters of both components. It may tell us about the internal structure for the pulsating star, especially for our Sun (Gough 2000). Therefore, it is important for us to probe such pulsations in helioseismology of eclipsing binaries (Aerts 2007; Huber 2015), which will help us to identify pulsating modes and compare the results from stellar theory. The pulsations of eclipsing binaries have not yet been adequately investigated, since the δ Scuti-type pulsations in AB Cas was first discovered by Tempesti (1971). In the detached and semi-detached binaries, mass transfer, accretion and gas envelopes may influence pulsation (Mkrtichian et al. 2005). Although the dozens of observed sample binaries (Liakos et al. 2012; Zhang et al. 2013; Yang et al. 2014), the problem of mode identification and shortcomings in the stellar models are majors difficulties (Pamyatnykh et al. 1998). The pulsation modes have been detected and their frequencies determined by many authors. Zhang et al. (2013) and Cakirli & İbanoğlu (2016) derived the correction between orbital and dominant pulsation periods. The threshold orbital period of ~ 13 day may be an apparent limit, beyond which the intrinsic pulsations for the δ Sct stars may not affected by the binarity (Liakos & Niarchos 2015). Liakos & Niarchos (2017) published the catalogue and properties of 118 δ Scuti stars in binaries. The pulsating binaries with less than 0.7 days are only two stars, i.e., VV UMa ($P = 0.6874$ day; Kim et al. 2005) and V1464 Aql ($P = 0.6978$ day; Dal & Sipahi 2013). Therefore, searching the short-period eclipsing binaries with pulsations is helpful for us to understand

their pulsating mechanisms.

EU Peg (=*2MASS* J23012519+2720211) is an Algol-type eclipsing binary with EA-type light curves (Budding et al. 2004). Malkov al. (2006) then classified it to be in "semi-detached status" and assigned its spectral type to be (A8)+[G2IV]. The visual magnitude ranges from 12.20 mag to 12.80 mag (Kukarkin et al. 1971). The orbital period of EU Peg is 0.7211 days, which is refined to be 0.721113 days (Keriner 2004). No determinations for this binary have been made of the physical properties, and the system then has generally neglected except for the measurements of the times of eclipse made up to now.

In this paper, we found a δ Scuti component in the EU Peg binary system, which is the third short-period pulsating binary. In Section 2, the photometry and spectroscopy for this binary are first presented. On the basis of two spectrograms, we determined the spectral type. Section 3 is devoted to study possible period variations. Modeling four-band light curves and pulsation analysis are given in Section 4, in which we obtained photometric elements and pulsating frequencies. Finally, we discussed the evolutionary state and causes of period changes.

2 Data and Their Reduction

2.1 Spectroscopy

Two low-resolution spectrograms for EU Peg were observed by using the *OMR* of the 2.16-m telescope at the Xinglong station (XLs) of National Astronomical Observatories of China (NAOC) on 2016 Oct 8, and the *BFOSC* of the 2.4-m telescope at the Lijiang station of Yunnan Astronomical Observatory (YNAO) on 2016 Oct 23, respectively. For the 2.16-m telescope, we chose the slit width of $1.''8$ and the *Grism-14* with a wavelength ranging from 3200 Å to 7500 Å (Fan et al. 2015). Its exposure time is 10 minutes. For the 2.4-m telescope, meanwhile, we used the grating of 1200 lines/mm, which results in the wavelength coverage $\sim$ 1380 Å (Fan et al. 2016). The exposure time is 15 minutes. Reduction of the spectra was performed by using IRAF packages [3], including bias subtraction, flat-fielding and cosmic-ray removal. Finally, the one-dimension spectrum was extracted. With the *winmk* software [4], two normalized spectra are displayed in Fig.1. The spectra of standard stars, HD 122408 and HD 002857 [5], are also plotted in both panels. The spectrum of Fig.1(a) is large noisy although the double lines for *Na* and $H\alpha$ line are evident. Due to lack of short wavelength, we re-observed this binary using the 2.4-m telescope and obtained the spectrum shown in Fig.1(b). On the basis of the stellar spectral classification (Gray & Corbally 2009), we determined its spectral type to be A3V, which differs from the estimated spectral type of (A8)+[G2IV] (Malkov al. 2006).

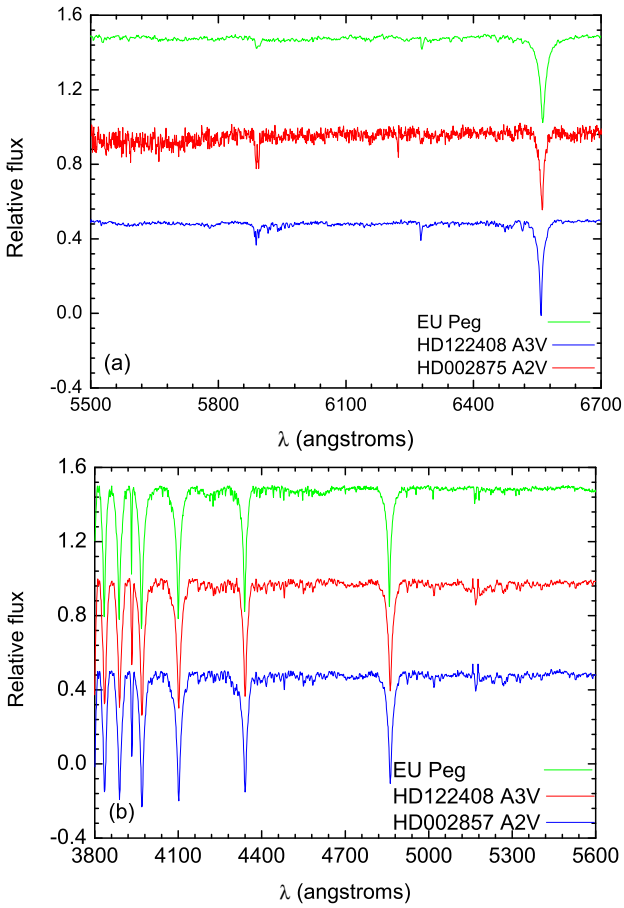

Fig. 1. Normalized spectra of the eclipsing binary EU Peg, which were observed on 2016 October 8 (a) and October 23 (b), respectively. The spectrum data are added the displacements of "+0.5" for HD 002857 and "-0.5" for HD 122408.

2.2 CCD Photometry

The comprehensive photometry for EU Peg was carried out from 2013 September 25 to November 11 with the 85-cm telescope (Zhou et al. 2009) and the 60-cm telescope (Yang et al. 2010) at XLs of NAOC. The standard Johnson-Cousin-Bessel $UBVR_cI_c$ systems are mounted on two small telescopes. Photometric effective images were reduced by using the IMRED and APPHOT packages in IRAF, after we preformed bias and dark subtraction, and flat-field correction. We then obtained the differential magnitudes between the variable and the comparison star.

In the observing process, TYC 2243-709-1 (*B=11.88, V=11.22*) and TYC 2243-1242-1 (*B=11.98, V=11.09*) are chosen to be the comparison and check stars, respectively. Typical exposure times were generally set to be 50s for B, 40 s for V,

[3] IRAF is supported by the National Optical Astronomy Observatories (NOAO) in Tucson, Arizona from http://iraf.noao.edu/iraf/web/iraf-homepage.html.
[4] http://www.appstate.edu/ grayro/MK/winmk.htm
[5] http://www.ast.obs-mip.fr/users/leborgne/stelib/stars.html

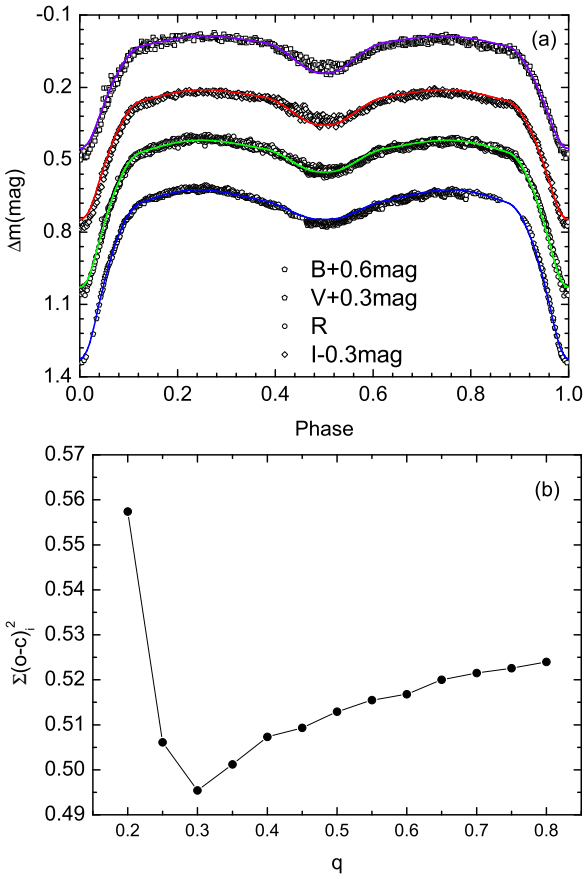

Fig. 2. BVR_cI_c-band light curves of EU Peg (a). The solid color lines are depicted by photometric solution (see from Table 5). The resulting $\Sigma(q)$ curve (b) is deduced from all photometric data.

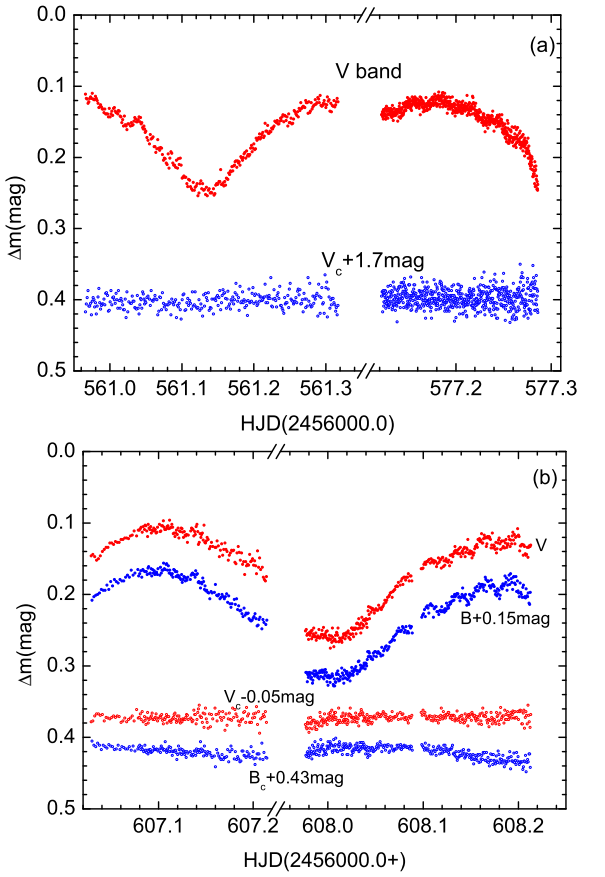

Fig. 3. Pulsating light variations with low amplitudes around secondary minima for EU Peg, observed by using the 85-cm telescope (a) and the 60-cm telescope (b) at XLs of NAOC in 2013. In low part of both panels, "Bc" and "Vc" values are in the sense of *Comparison-Check* with magnitude displacements.

30 s for R_c and 25 s for I_c band, which depends on the weather condition. Most useful observations were obtained on 9 nights. In total, we obtained 4565 effective CCD images. Table 1 lists heliocentric Julian dates (HJDs) *versus* differential magnitudes with respect to the comparison star. The $Comparison-Check$ magnitude differences, i.e., *rms* scatters, are 0.007 mag in B and 0.006 mag in V band for the 60-cm telescope, and 0.013 mag in V, 0.014 mag in R_c, and 0.022 in I_c band for the 85-cm telescope, respectively. The complete light curves are shown in Fig.2(a), in which phases are computed by the new linear ephemeris in Eq.(1) in Sect.3. From this figure, the brightness fluctuations, especially in B and V bands, occur during the secondary minima and disappear near the central phase of the primary minima, which is similar to another previously studied star FR Ori (Yang et al. 2014). The low-amplitude pulsations in BV light curves are displayed in Fig.3, which are obtained only at the fine nights. The pulsations occurring at the secondary eclipses imply that the more massive component in the EU Peg binary may be a δ Scuti-type star.

3 Orbital Period Variations

From our new data, we determined four light minimum times, listed in Table 2. From the *O-C* gateway [6], a total of 34 eclipse times (i.e., 11 photographic, 3 photoelectric and 20 CCD ones) was compiled to study the period changes. Table 3 give those data with their errors and measured methods. For all eclipsing times, individual weights are assigned inversely proportional to their standard errors. However, the uncertainties for some timings did not be given. Therefore, we assumed the errors of ±0.001 day for 11 photographic data, and ±0.0005 day for 2 photoelectric ones (Hübscher et al. 1994), respectively. Based on all times of minimum light, a weight least-squares method yields a new linear ephemeris as follows,

$$\mathrm{Min.\,I} = \mathrm{HJD}\ 2456562.2086(11) + 0.72111515(8) \times \mathrm{E}, \quad (1)$$

in which the number in brackets are listed the errors in the last decimal place. Initial timing residuals with respect to Eq.(1), $(O-C)_i$, are listed in Table 3 and displayed in Fig.4(a). From

[6] http://var2.astro.cz/ocgate/

this figure, the orbital period of EU Peg clearly displays a secular decrease with some irregular oscillations, although a 36-year gap exists between HJD 2435401.078 (Kaho 1952) and HJD 2448465.538 (Hübscher et al. 1995). Therefore we assumed that the $(O-C)_i$ curve may be described by a downward parabola with a sinusoidal curve, whose is similar to the case occurring in the binary SX Dra (Soydugan & Kaçar 2013). By using a nonlinear least-squares method with weights, the following equation was used to represent the cyclic variation and parabola of the $(O-C)$ data,

$$\mathrm{Min.\ I} = \mathrm{T_0} + \mathrm{P}\times\mathrm{E} + \mathrm{Q}\times\mathrm{E}^2 + \mathrm{A_{mod}}\times\sin[\frac{2\pi}{\mathrm{P_{mod}}}(\mathrm{E}-\mathrm{T_s})], \quad (2)$$

where A_{mod}, P_{mod} and T_s are the amplitude, period and moment of the minimum of sinusoidal variation, while T_0, P, Q and E are the epoch , orbital period of the binary system, the coefficient of quadratic term and epoch number, respectively. The fitting parameters are listed in Table 4. From Eq.(2), we obtained the computed values, $(O-C)_{\mathrm{parab}}$ and $(O-C)_{\mathrm{c}}$, for all eclipsing times, which are listed in Table 3. From the coefficient of quadratic term, Q, we determined a period decrease rate of $dP/dt = -7.34(\pm1.06)\times10^{-7}$ day/yr. As shown in Fig.4(a), the solid and dotted lines are plotted by Eq.(2) and only its parabolic part, respectively.

After removed from $(O-C)_i$ by the best parabolic fit of Eq.(2), the $(O-C)_c$ residuals are displayed in Fig.4(b). The cyclic change is plotted as a solid line only by the sinusoidal term of Eq.(2). The period of this oscillation is $P_{mod} = 31.0(\pm1.4)$ yr. From the fit including both quadratic and sinusoidal terms, we obtained the final residuals $(O-C)_f$, which are listed in Table 3 and shown in Fig.4(c). From this figure, no regularity is found. Therefore, Eq.(2) is acceptable for us to fit all data, although a large gap exists. In the future observation, more eclipsing times are needed to check the behavior of the orbital period variations.

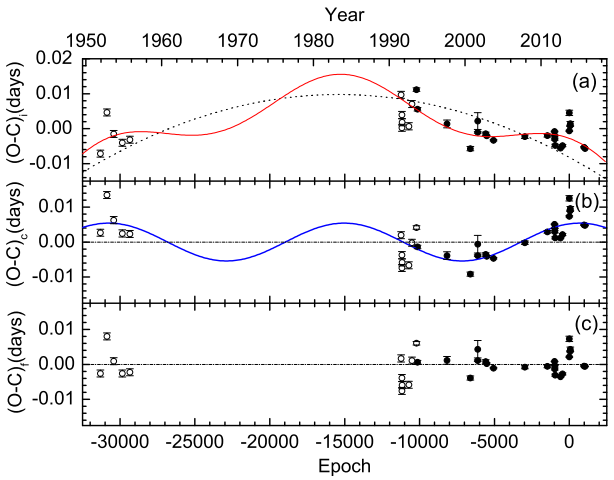

Fig. 4. The residual diagrams: $(O-C)_i$ (a), $(O-C)_c$ (b), and $(O-C)_f$ (c). The open and filled circles represent photographic measurements, and photoelectric/CCD ones, respectively. In the panel (a), the solid and dotted lines are computed by Eq.(2) and only its parabolic part, respectively. Meanwhile, the continuous curve in the panel (b) is plotted by the sinusoidal term of Eq.(2).

4 Analyzing Light Curves

From the light curves of Fig.2(a), EU Peg is identified to be an Algol-type eclipsing binary. The photometric elements are deduced from four-color light curves, including 912 data in B band, 2729 in V band, 806 in R_c band and 741 in I_c band. After the binary solution was removed from the observations (i.e., the light-curve residuals), a Fourier analysis was performed on the residuals in order to study the pulsation behavior of the primary component.

4.1 Photometric Solution

Theoretical light curves of EU Peg were simultaneously computed by the 2015-version W-D Program (Wilson & Devinney 1971; Wilson & Van Hamme 2014) [7]. The limb darkening coefficients are generated with the LC and DC programs. In the calculating process, we fixed $LD_1 = LD_2 = -2$ for the bolometric logarithmic limb darkening law (van Hamme & Wilson 2007), and MREF=2 for the detailed reflect model (Wilson 1979). Assumed the spectral type of A3V with an uncertainty of a subtype for EU Peg, the mean effective temperature for Star 1 may be estimated to be $T_1 = 8730(\pm270)$ K, which are based on the calibration of *MK* spectral types (Cox 2000). The gravity darking exponents and bolometric albedo coefficients are fixed to be $g_1 = 1.0$ (von Zeipel 1924) and $g_2 = 0.32$ (Lucy 1967), $A_1 = 1.0$ and $A_2 = 0.5$ (Rucinski 1973), respectively. As usual, other adjustable parameters are T_0, P_0, T_2, i, q, Ω_1, Ω_2 and ℓ_3 in solving light curves.

In order to search a mass ratio, we performed a q-search process from all data. The tried solutions imply that EU Peg has a detached configuration, rather than a semi-detached one (Budding et al. 2004). The relation between q and Σ is shown in Fig.2(b), in which a minimum value of Σ arrives around a mass ratio of 0.3. The mass ratio q and third light ℓ_3 are then considered to be free parameters. The final photometric elements are listed in Table 5. The fill-out factor is computed by $f = < r > /r_{cr}$, in which r_{cr} is an equivalent relative radius of Roche lobe (Eggleton 1983). The values for both components are $f_p = 86.7(\pm0.6)\%$ and $f_s = 92.6(\pm0.1\%)$. The computed light curves are plotted as solid lines in Fig.2(a). From this figure, R_c and I_c light curves may be not fitted well, which may be contributed the different filters. The contributions to the total light, ℓ_3, are 0.25%, 0.39% and 0.68% in B, V, R_c and I_c

[7] FTP site: //ftp.astro.ufl.edu/pub/wilson/lcdc2015.

bands, respectively.

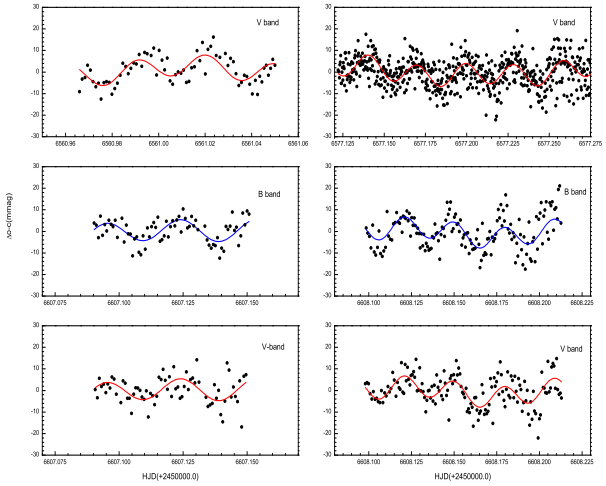

Fig. 5. Residual light curves with pulsations, observed by using the 85-cm telescope (*top*), and the 60-cm telescope (*middle* and *bottom*). The solid lines are plotted by three fitted frequencies from Table 6.

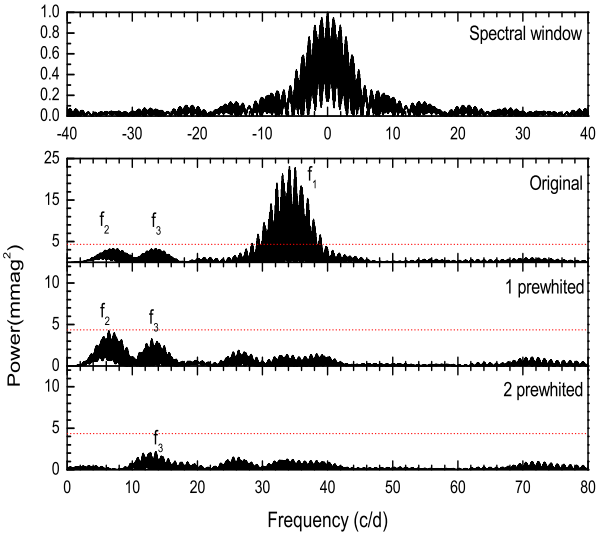

Fig. 6. Spectral window, power spectra and significance limit (as dotted line), which are derived from all pulsating data in B and V.

4.2 Pulsating Frequency Analysis

To explore pulsating frequencies, small-amplitude pulsations were analyzed after removed by the binary solution from light curves. From Fig.3, the pulsations occur around both light maxima, which may result from the more massive component, possibly in the instability strip of H-R diagram. This kind of pulsations occur in other short-period ($P < 1$ days) detached Algol-type binary HZ Dra (Liakos et al. 2012). After the eclipses and proximity effects of the binary were removed by theoretical light curves, we obtained 5.9 hr in V band (from the 85 telescope), and 4.2 hr in B, V bands (from the 60-cm telescope) residual data. Due to only 10.1-hour pulsations (i.e., 225 in B band and 917 in V band), searching pulsation frequencies is then preliminary. As shown in Fig.5, a total of 1142 residual observations were analyzed by using Period04 software [8] (Lenz 2004; Lenz & Breger 2005), which is based on the classical discrete Fourier transform and multiple-least-squares algorithms.

When we calculate frequencies, the residual light curves were subsequently pre-whitened one by one. The signal/noise amplitude ratio is $S/N \sim 4.0$ as a good criterion to distinguish between peaks due to pulsation and noise (Breger et al. 1993). The analyses were preformed for B data, V data, and all data together, respectively. The detected frequencies are listed in Table 6, in which the uncertainties of parameters are computed by the formulae from Montgomery & O'donoghue (1999). The observed noises are $\sigma(m)_B = 0.0071$ mag, $\sigma(m)_V = 0.0113$ mag and $\sigma(m)_{B+V} = 0.0106$ mag, respectively. From Table 5, three frequencies from V data approximately agree with those from all data. For 225 data in B band, the only reliable result may be the frequency of f_1. So we accept the results derived from the data in B and V bands. The spectral window and amplitude spectra are displayed in Fig.6, although three peaks are not prominent due to pulsating observations with a short duration of 10.1 hours. Using the estimated parameters in Table 4, the mean density of the primary can be computed to be $\rho_1/\rho_\odot = \frac{M_1}{M_\odot}/(\frac{R_1}{R_\odot})^3 = 0.2685(\pm 0.0370)$. Following the formula of $Q = P_{pul}(\rho/\rho_\odot)$, we can calculate the pulsating constant for each frequency. The theoretical curves are plotted in Fig.5 as solid lines by using the equation of $m(t) = a_0 + \sum a_i \sin[2\pi(f_i t + \phi_i)]$ $(i = 1, 2, 3)$, where $m(t)$, a_0, a_i, ϕ_i and f_i are calculated magnitude, zero point, semi-amplitude, phase and frequency of the i-th frequency. The dominant frequency of $f_1 = 34.119$ c/d (i.e., $P_{puls} \simeq 42.2$ minutes) with an amplitude of $4.82(\pm 0.44)$ mmag may be a reliable pulsating frequency. The value of Q for low-radial-order press mode (i.e., p-mode) oscillation of a δ-Scuti star is shorter than 0.04 day or less (Handler & Shobbrook 2002), which serves as a criterion to perform a rough-mode identification. In order to further identify the pulsation mode, we estimated phase shift and amplitude ratio between B and V bands. For the frequency of f_1 from Table 5, the observed phase shift is +4.6° for B-V, which means its radial pulsation according to the diagrams of Watson (1988) and Garrido et al. (1996). The amplitude ratio of B/V of 1.47 may be a typical value compared with those for radial mode δ Scuti stars (Rodríguez et al. 1996). Therefore, the detected frequency of f_1 may be a p-mode pulsator.

Based on the eclipsing binaries with δ Scuti type primaries, Soydugan et al. (2006) and Soydugan & Kaçar (2013) successively derived two relations of $P_{puls} - P_{orb}$ (see Fig.7a) and $\log P_{plus} - \log F$ (see Fig.7b), where F is the gravitational pull

[8] Period04 is available at the web site of http://www.univie.ac.at/tops/.

exerted to per gram of the matter on the surface of the primaries by the secondary companions. The primary pulsation of EU Peg (i.e., $P_{\rm plus} = 0.029$ days) is also plotted as a solid circle in Fig.7. From both panels, the observed main pulsation of EU Peg identifies the two relations (Soydugan et al. 2006; Soydugan & Kaçar 2013). For the short-period Algol-type binary EU Peg, the large gravitational force exerted from the secondary component, F, results in the short pulsating period. Figure 7 implies that when the orbital period decreases, the separation between two components decreases. This will cause the gravitational force applied by the secondary companion onto the pulsating primary star to increase. Finally, the pulsating period will also decrease. According to the criterion given Breger et al. (1993), two frequencies f_2 and f_3 are below the significance limit and maybe are not meaningful. This case occurs in the pulsating binary SX Dra (Soydugan & Kaçar 2013). Therefore, f_2, and f_3 with low amplitudes are needed to further identify in the future.

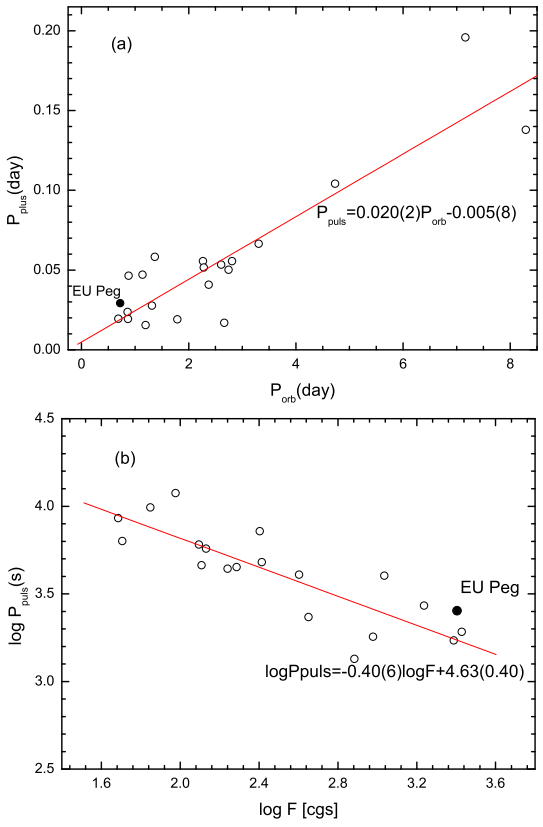

Fig. 7. (a)The relation between P_{orb} and P_{puls} taken from Soydugan et al. (2006), where the open circles represent 20 systems. (b) The relation between P_{orb} and P_{puls} taken from Soydugan & Kaçar (2013), in which the open circles refer to 19 binaries. The solid circle refers to the binary EU Peg in both panels.

5 Discussions

From the previous analysis, EU Peg is a detached binary with a δ Sculti component, whose mass ratio is $q = 0.3105(\pm 0.0011)$. The fill-out factors for both components are $f_p = 86.7(\pm 0.6)\%$ and $f_s = 92.6(\pm 0.1)\%$, respectively. The light curves process small pulsations, The dominant pulsating frequency of $f_1 = 34.12$ c/d is a p-mode pulsation. In order to reliable frequency values, more data are needed in the future observation. Due to the lack of spectroscopic elements (i.e., the semi-amplitudes of radial velocity curves, K_1 and K_2), the absolute parameters are estimated by using Kepler's third law, $M_1 + M_2 = 0.134a^3/P^2$, in which $M_{1,2}$, a and P are in units of $M_\odot$, $R_\odot$ and day respectively.

Based on the spectral type of A3V assuming with a subtype error, we adopted a mass of $M_1 = 2.60(\pm 0.30)$ $M_\odot$ (Cox 2000). Using the Kepler's third law and photometric solution, we determined other absolute parameters, listed in Table 5. In Both components are shown in Fig.8. *ZAMS, TAMS*, evolutionary tracks and isochrones for solar chemical compositions are taken from Girardi et al. (2000). The primary component between ZAMS and TAMS lines, is close to ~ 2.0 $M_\odot$ in an isochrone of ~ 0.47 Gyr, whose low luminosity and temperature with respect to its mass may result from the single-star evolutionary model. Meanwhile, the secondary component is near to the evolutionary track of 0.8 $M_\odot$, and is far from the isochrone line. This may result form the binary interactive, which may represent its true evolutionary state.

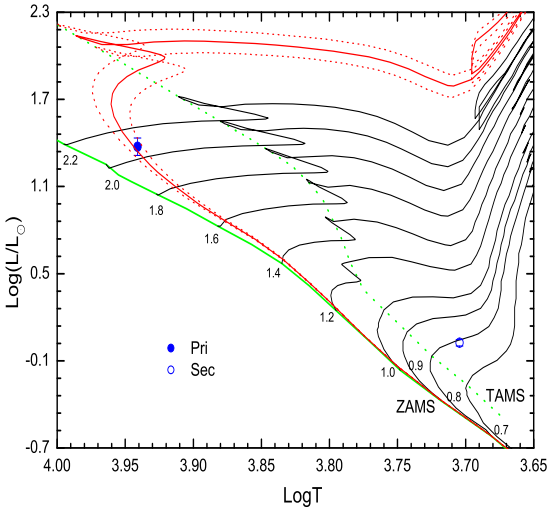

Fig. 8. The evolutionary locations of both components for the detached binary EU Peg.

From the period analysis, the $(O-C)$ curve possibly includes a cyclic variation. For the close binaries, this kind of changes may be attributed to either cyclic magnetic activity (Applegate 1992) or light-time effect (Irwin 1952). For the early-type binary EU Peg, the less massive component may be

an active star. The observed amplitude of sinusoidal term in Eq.(2) may result from the change of gravitational quadrupole moment, which can be computed by Lanza & Rodonò (2002)'s equation as follows,

$$-9\frac{R}{a}\frac{\Delta Q}{MR^2}=\frac{\Delta P}{P}\simeq\frac{2\pi A_{mod}}{P_{mod}}, \tag{3}$$

where a, R, M are taken from Table 5, A and P_{mod} from Eq.(2), respectively. The value of $\Delta Q_2=6.71(\pm1.24)\times10^{-49}$ g cm^2 is much smaller than the typical order of $10^{-51}-10^{-52}$ g cm^2 (Lanza & Rodonò 1999). Therefore, we could remove the magnetic active, which may not work out in the secondary. On the other hand, another mechanism is light-time effect due to the assumed third companion. From Eq.(2), we can easily obtain the value of $a_{12}\sin i'=A_{mod}\times c$, in which c and i' are light velocity and orbital inclination. Then we can compute the mass function of the additional companion, $f(m)$, with the help of the following equation,

$$f(m)=\frac{4\pi^2}{GP_{mod}^2}\times(a_{12}\sin i')^3=\frac{(M_3\sin i')^3}{(M_1+M_2+M_3)^2}. \tag{4}$$

By the iteration method, we can determine the mass and radius for some an orbital inclination i'. The minimum mass for the suggested third companion (i.e., $i'=90$ deg) is $M_3=0.23(\pm0.04)$ M$_\odot$ at a radius of $14.2(\pm5.1)$ AU. It may be a red dwarf with low luminosity (i.e., $\ell_3\leq1.0\%$), which is difficult to explore by spectroscopy.

In the non-conservative evolution for a close binary, the secular period changes should be the result of a net effect of mass transfer, mass loss, and angular momentum loss (Tout & Hall 1991). Due to the detached configuration for EU Peg, both components do not fill the Roche lobes, respectively. Assuming that the mass loss due to stellar wind is proportional to its total mass of system (i.e., $\dot{M}=\dot{M}_2M/M_2$) and the escape radius is equal to the separation between both components (i.e., $R_{es}\simeq a$), we can obtain a simplified formula as follows (see Yang et al. 2013),

$$\frac{1}{P}\frac{dP}{dt}=\frac{5q^2-q+2}{q}\frac{\dot{M}}{M}, \tag{5}$$

where P, q, M are orbital period, mass ratio and total mass, respectively. Inserting dP/dt and other parameters of the binary, we can determine a mass loss rate of $dM/dt=-4.96(\pm0.72)\times10^{-8}$ M$_\odot$/yr. Moreover, the possible additional companion in the EU Peg binary may extract angular momentum from the central system. Mass loss and angular loss result in the period decreasing. This will cause the orbit of binary to shrink. Due to two components nearly filling their limiting Roche lobes, EU Peg finally may evolve from the detached configuration into the semi-detached one. More high-precision spectroscopy and photometry for EU Peg are necessitated to determine the absolute parameters more reliably, to explore the pulsating frequencies and to search any signature of the presence of a third component.

This research is partly supported by Natural Science Foundation of China (grant Nos. 11473009 and U1231102), and Natural Science Research Project of Anhui Provincial Department of Education (grant No. KJ2017A850). Dr Yuangui Yang thanks Prof. Aigen Li for his invitation to collaborate on the study on the planet-forming dust disks at the University of Missouri as a senior visiting scholar. Low-precision spectra are observed by the 2.4-m telescope at Lijiang station of YNAO and the 2.16-m telescope at XLs of NAOC. Many thanks are given to Professor Qing-Zhong Liu for his providing the observing time of 2.16-m telescope. The comprehensive photometry was carried out by the 60-cm and 85-cm telescopes at XLs of NAOC. We also made extensive use of the *Simbad* and NASA ADS databases.

References

Aerts, C., 2006, IAUS, 240, 432
Agerer, F., & Hübscher, J., 1999, Inf. Bull. Var. Stars, 4712, 1
Agerer, F., & Hübscher, J., 2003, Inf. Bull. Var. Stars, 5484, 1
Applegate, J. H., 1992, ApJ, 385, 621
Breger, M., Stich, J., Garrido, R., et al., 1993, A&A, 271, 482
Budding, E., Erdem, A., Çiçek, C., et al., 2004, A&A, 417, 263
Cakirli, Ö., & İbanoğlu, C., 2016, New Astron., 45, 36
Cox, A. N. 2000, Allen's Astrophysical Quantities, 4th ed. (New York: Springer)
Diethelm, R., 2000, BBSAG Bull, 123, 1
Diethelm, R., 2003, Inf. Bull. Var. Stars, 5438, 1
Diethelm, R., 2011, Inf. Bull. Var. Stars, 5960, 1
Diethelm, R., 2012, Inf. Bull. Var. Stars, 6011, 1
Diethelm, R., 2013, Inf. Bull. Var. Stars, 6042, 1
Dal, H. A., & Sipahi, E., PASA, 30, 16
Dvorak, S. W., 2003, Inf. Bull. Var. Stars, 5378, 1
Eggleton, P. P., 1983, ApJ, 268, 368
Fan, Yu-Feng, Bai, Jin-Ming, Zhang, Ju-Jia, et al., 2015, RAA, 15, 918
Fan, Zhou, Wang, Huijuan, Jiang, Xiaojun, et al., 2016, PASP, 128, 115005(15pp)
Garrido, R., Garcia-Lobo, E., & Rodríguez, E., 1990, A&A, 234, 262
Girardi, L., Bressan, A., Bertelli, G., & Chiosi, C., 2000, A&AS, 141, 371
Gray, R. O., & Corbally, C. J., 2009, Stellar spectral classification, Princeton Univ. Press (New Jersey: Princeton)
Gough, D., 2000, ASPC, 203, 529
Handler, G., & Shobbrook, R. R., 2002, MNRAS, 333, 251
Hübscher, J., 2005, Inf. Bull. Var. Stars, 5643, 1
Hübscher, J., 2014, Inf. Bull. Var. Stars, 6118, 1
Huber, D., 2015, Astrophysics and Space Science Library, 408, 169
Hübscher, J., Agerer, F., & Wunder, E., 1992, BAV Mitt., 60, 1
Hübscher, J., Agerer, F., & Wunder, E., 1993, BAV Mitt., 62, 1
Hübscher, J., Agerer, F., & Wunder, E., 1994, BAV Mitt., 68, 1
Hübscher, J., Agerer, F., & Wunder, E., 1995, BAV Mitt., 79, 1
Hübscher, J., Agerer, F., & Wunder, E., 1996, BAV Mitt., 93, 1
Irwin, J. B., 1952, ApJ, 116, 211
Juryšek, J. Hoňková, K., Šmelcer, L., et al., 2017, Open Eur. J. Var. Stars, 179, 1
Kaho, S., 1952, Tokyo Bull. Sec. Ser., 30, 217

Kim, S.-L., Lee, J. W., Lee, C.-U., et al., 2005, Inf. Bull. Var. Stars, 5598, 1
Kreiner, J. M., 2004, Acta Astron., 54, 207
Kreiner, J. M., 2011, private communciation
Kukarkin, B. V., Kholopov, P. N., Pskovsky, Y. P., et al., 1971, General Catalogue of Variable Stars, 3rd ed.
Liakos, A., & Niarchos, P., 2015, in Rucinski, S. M., Torres, G., Zejda, M., eds, ASP Conf. Ser., Vol. 496, Living Together: Planets, Host Stars and Binaries, Astron. Soc. Pac. San Francisco, p.195
Liakos, A., & Niarchos, P., 2017, MNRAS, 465, 1181
Lanza, A. F., & Rodonò, M., 1999, A&A, 349, 887
Lanza, A. F., & Rodonò, M., 2002, Astron. Notes, 323, 424
Lenz, P., 2004, Comm. in Asteroseismology, 144, 41
Lenz, P., & Breger, M., 2005, Comm. in Asteroseismology, 146, 1
Liakos, A., Niarchos, P., Soydugan, E., & Zasche, P., 2012, MNRAS, 422, 1250
Lucy, L. B., 1967, ZA, 65, 89
Malkov, Y. O., Oblak, E., Snegireva, E. A., & Torra, J., 2006, A&A, 446, 785
Montgomery, M. H., & O'donoghue, D., 1999, Delta Scuti Star Newsletter, 13, 28
Mkrtichian, D. E., Rodríguez, E., Olson, E. C., et al., 2005, ASPC, 333, 197
Nagai, K., 2008, Var. Star Bull. Japan, 46, 1
Pickles, A., & Depagne, E., 2010, PASP, 122, 1437
Pamyatnykh, A. A., Dziembowski, W. A., Handler, G., & Pikall, H., 1998, A&A, 331, 141
Rodríguez, E., Rolland, A., López de Coca, P., & Martín, S., 1996, A&A, 307, 539
Rucinski, S. M., 1973, Astron. Acta, 23, 79
Soydugan, E., İbanoğlu, C., Soydugan, F., et al., 2006, MNRAS, 366, 1289
Soydugan, E., & Kaçar, Y., 2013, AJ, 145, 87 (8pp)
Tempesti, P., 1971, Inf. Bull. Var. Stars, 596, 1
Tout, C. A., & Hall, D. S., 1991, MNRAS, 253, 9
van Hamme, W., & Wilson, R. E. 2007, ApJ, 661, 1129
von Zeipel, H., 1924, MNRAS, 84, 655
Watson, R. D., 1988, Ap&SS, 140, 255
Wilson, R. E., 1979, ApJ, 234, 1054
Wilson, R. E., & Devinney, E. J. 1971, ApJ, 166, 605
Wilson, R. E., & Van Hamme, W. 2014, ApJ, 780, 151
Yang, Y.-G., Dai, H.-F., & Yin, X.-G., 2010, New Astron., 15, 392
Yang, Y.-G., Qian, S.-B., & Dai, H.-F., 2013, AJ, 145, 60
Yang, Y.-G., Wei, J.-Y., & Li, H.-L., 2014, AJ, 147, 35
Zejda, M., 2004, Inf. Bull. Var. Stars, 5583, 1
Zhang, X.-B., Luo, C.-Q., & Fu, J.-N., 2013, ApJ, 777, 77
Zhou, A.-Y., Jiang, X.-J., Zhang, Y.-P., & Wei, J.-Y., 2009, Res. Astron. Astrophys., 9, 349

Table 1. Multicolor Photometric Observations for EU Peg

60-cm telescope				85-cm telescope					
B band		V band		V band		R_c band		I_c band	
JD(Hel.)	Δm	JD(Hel.)	Δm	JD(Hel.)	Δm	JD(Hel.)	Δm	JD(Hel.)	Δm
601.98744	+0.053	576.15711	+0.126	560.96598	+0.111	560.96656	+0.214	561.05232	+0.330
601.98868	+0.051	576.15750	+0.126	560.96715	+0.117	560.96773	+0.218	561.05362	+0.324
601.98992	+0.044	576.15790	+0.125	560.96831	+0.118	560.96890	+0.219	561.05558	+0.327
601.99116	+0.050	576.15829	+0.121	560.96948	+0.124	560.97006	+0.224	561.05689	+0.348
601.99258	+0.046	576.15869	+0.133	560.97065	+0.122	560.97123	+0.221	561.05819	+0.339
601.99405	+0.048	576.15908	+0.130	560.97181	+0.117	560.97238	+0.216	561.05949	+0.343
601.99552	+0.056	576.15948	+0.127	560.97297	+0.115	560.97355	+0.214	561.06079	+0.352
601.99699	+0.048	576.15987	+0.138	560.97413	+0.117	560.97472	+0.220	561.06209	+0.342
601.99847	+0.043	576.16026	+0.129	560.97530	+0.110	560.97588	+0.213	561.06339	+0.341
601.99997	+0.048	576.16066	+0.124	560.97647	+0.118	560.97705	+0.222	561.06468	+0.354
602.00148	+0.036	576.16105	+0.127	560.97763	+0.119	560.97822	+0.217	561.06599	+0.338
602.00300	+0.044	576.16145	+0.124	560.97880	+0.119	560.97938	+0.221	561.06729	+0.352

Notice: All individual data are available only on the web journal of *PASJ*.

Table 2. New Observed Eclipsing Times for EU Peg

JD(Hel.)	Error	Filter	Min.	Telescopes
2456561.13335	±0.00065	V	II	85-cm
2456561.13790	±0.00100	R_c	II	85-cm
2456561.13238	±0.00066	I_c	II	85-cm
2456562.21142	±0.00023	V	I	85-cm
2456562.20989	±0.00019	R_c	I	85-cm
2456562.21184	±0.00023	I_c	I	85-cm
2456604.03722	±0.00019	B	I	60-cm
2456606.20108	±0.00057	B	I	60-cm
2456606.20121	±0.00069	V	I	60-cm

Table 3. All Available Times of Light Minima for EU Peg

JD(Hel.)	Error	Epoch	Method	$(O-C)_i$ (days)	$(O-C)_{\rm parab}$ (days)	$(O-C)_{\rm c}$ (days)	$(O-C)_f$ (days)	References
2433981.919[a]	±0.001	−31313.0	pg	−0.0109	−0.0136	+0.0053	−0.0026	Kaho (1952)
2434302.106[a]	±0.001	−30869.0	pg	+0.0009	−0.0125	+0.0054	+0.0080	Kaho (1952)
2434628.044[a]	±0.001	−30417.0	pg	−0.0051	−0.0114	+0.0054	+0.0009	Kaho (1952)
2435044.125[a]	±0.001	−29840.0	pg	−0.0076	−0.0100	+0.0051	−0.0026	Kaho (1952)
2435401.078[a]	±0.001	−29345.0	pg	−0.0066	−0.0089	+0.0046	−0.0022	Kaho (1952)
2448465.538[a]	±0.001	−11228.0	pg	+0.0103	+0.0083	+0.0003	+0.0017	Hübscher et al. (1995)
2448499.421[a]	±0.001	−11181.0	pg	+0.0009	+0.0083	+0.0002	−0.0076	Hübscher et al. (1992)
2448501.588[a]	±0.001	−11178.0	pg	+0.0045	+0.0083	+0.0002	−0.0039	Hübscher et al. (1992)
2448514.566[a]	±0.001	−11160.0	pg	+0.0024	+0.0083	+0.0001	−0.0060	Hübscher et al. (1992)
2448840.509[a]	±0.001	−10708.0	pg	+0.0014	+0.0081	−0.0008	−0.0058	Hübscher et al. (1996)
2448988.344[a]	±0.001	−10503.0	pg	+0.0078	+0.0080	−0.0013	+0.0011	Hübscher & Agerer (1993)
2449202.5194[b]	±0.0005	−10206.0	pe	+0.0120	+0.0078	−0.0019	+0.0060	Hübscher et al. (1994)
2449249.3863[b]	±0.0005	−10141.0	pe	+0.0064	+0.0078	−0.0020	+0.0006	Hübscher et al. (1994)
2450671.4216	±0.0011	−8169.0	CCD	+0.0026	+0.0065	−0.0050	+0.0011	Agerer & Hübscher (1999)
2451796.3545	±0.0006	−6609.0	CCD	−0.0041	+0.0051	−0.0053	−0.0039	Diethelm (2000)
2452147.5456	±0.0024	−6122.0	CCD	+0.0039	+0.0045	−0.0049	+0.0043	Zejda (2004)
2452150.4268	±0.0002	−6118.0	CCD	+0.0007	+0.0045	−0.0049	+0.0011	Agerer & Hübscher (2003)
2452535.5020	±0.0005	−5584.0	CCD	+0.0004	+0.0039	−0.0044	+0.0008	Diethelm (2003)
2452581.6528	±0.0002	−5520.0	CCD	−0.0002	+0.0038	−0.0043	+0.0002	Dvorak (2003)
2452913.3646	±0.0002	−5060.0	CCD	−0.0014	+0.0033	−0.0036	−0.0011	Hübscher (2005)
2454421.9390	±0.0005	−2968.0	CCD	+0.0001	+0.0003	+0.0006	−0.0008	Nagai (2008)
2455500.7279	±0.0004	−1472.0	CCD	+0.0008	−0.0022	+0.0035	−0.0006	Diethelm (2011)
2455854.7967	±0.0001	−981.0	CCD	+0.0020	−0.0031	+0.0042	+0.0008	Kreiner (2011)
2455862.7278	±0.0001	−970.0	CCD	+0.0009	−0.0031	+0.0043	−0.0003	Kreiner (2011)
2455863.8085	±0.0003	−968.5	CCD	−0.0001	−0.0031	+0.0043	−0.0013	Kreiner (2011)
2455875.7051	±0.0003	−952.0	CCD	−0.0019	−0.0031	+0.0043	−0.0031	Diethelm (2012)
2456132.4214	±0.0002	−596.0	pe	−0.0026	−0.0038	+0.0047	−0.0035	Hübscher (2014)
2456232.6571	±0.0003	−457.0	CCD	−0.0019	−0.0040	+0.0049	−0.0027	Diethelm (2013)
2456561.1345	±0.0008	−1.5	CCD	+0.0076	−0.0049	+0.0052	+0.0073	Present paper
2456562.2111	±0.0002	+0.0	CCD	+0.0024	−0.0049	+0.0052	+0.0022	Present paper
2456604.0372	±0.0002	+58.0	CCD	+0.0039	−0.0051	+0.0052	+0.0037	Present paper
2456606.2012	±0.0006	+61.0	CCD	+0.0045	−0.0051	+0.0052	+0.0043	Present paper
2457267.4572	±0.0002	+978.0	CCD	−0.0021	−0.0070	+0.0054	−0.0005	Juryšek et al. (2017)
2457324.4250	±0.0001	+1057.0	CCD	−0.0023	−0.0071	+0.0054	−0.0006	Juryšek et al. (2017)

Notice: [a]For 11 photographic data, we assumed their observed errors to be ±0.001 day.

[b]For two photoelectric data (Hübscher et al. 1995), their uncertainties are given to be ±0.0005 day.

Table 4. New ephemeris of EU Peg

Quadratic plus sinusoidal fitting
Min.I (HJD)=$T_0 + E \times P + Q \times E^2 + A \times \sin[\frac{2\pi}{P_{mod}}(E - T_s)]$
T_0=HJD 2456562.2037($\pm$0.0008)
P=0.72111515($\pm$0.00000028) d
Q=$-7.24(\pm1.05) \times 10^{-11}$ d
A_{mod}=0.0054($\pm$0.0010) d
$P_{mod} = 11327(\pm570)$ days=31.0($\pm$1.4) years
$T_s = 12470(\pm400)$ epochs

Table 5. Geometrical and Physical Parameters for EU Peg

Parameter	Primary	Secondary
T (K)	8730 ± 270^a	5064 ± 12
T_0(HJD)	$2456562.2117(\pm0.0002)$	
P_0(day)	$0.72113316(\pm0.00000192)$	
i (deg)	81.3 ± 0.8	
$q = M_2/M_1$	0.3105 ± 0.0011	
$\Omega_{1,2}$	2.8713 ± 0.0031	2.5938 ± 0.0041
$L_i/(L_1+L_2)_B$	0.9829 ± 0.0055	0.0171
$L_i/(L_1+L_2)_V$	0.9650 ± 0.0057	0.0350
$L_i/(L_1+L_2)_{R_c}$	0.9474 ± 0.0065	0.0526
$L_i/(L_1+L_2)_{I_c}$	0.9269 ± 0.0087	0.0731
$\ell_{3B}(\%)$	0.25 ± 0.04	
$\ell_{3V}(\%)$	0.39 ± 0.04	
$\ell_{3R_c}(\%)$	0.68 ± 0.05	
$\ell_{3I_c}(\%)$	1.02 ± 0.07	
r(pole)	0.3954 ± 0.0022	0.2429 ± 0.0018
r(point)	0.4398 ± 0.0035	0.2875 ± 0.0087
r(side)	0.4134 ± 0.0034	0.2506 ± 0.0020
r(back)	0.4256 ± 0.0025	0.2714 ± 0.0023
$< r >^b$	0.4185 ± 0.0032	0.2631 ± 0.0037
a ($R_\odot$)	5.09 ± 0.20	
M ($M_\odot$)	2.60 ± 0.30^c	0.81 ± 0.10
R ($R_\odot$)	2.13 ± 0.02	1.34 ± 0.02
L ($L_\odot$)	23.65 ± 0.36	1.06 ± 0.03

Notice: [a]The mean effective temperature for the more massive component is fixed from the spectral type of A3V with an uncertainty of a subtype.

[b]Bracket indicates the equal-volume radius.

[c]Based on A3V with a subtype error, the mass for the primary component (i.e., star 1) was estimated (Cox 2000).

Table 6. Results of the Multiple-Frequency Analysis

Band	Frequency (c/d)	Amplitude (mmag)	Phase (rad)	S/N	Q ($\times 10^{-2}$ days)
B	$f_1 = 34.125436(3)^a$	6.55 ± 0.67	0.9784 ± 0.1025	7.927	1.52
	$f_2 = 11.182094(9)$	1.74 ± 0.67	0.5956 ± 0.3860	4.152	4.63
V	$f_1 = 34.183144(3)$	4.47 ± 0.53	0.8968 ± 0.1176	13.365	1.52
	$f_2 = 6.455440(5)$	2.17 ± 0.53	0.9837 ± 0.2423	12.436	8.03
	$f_3 = 12.904531(7)$	1.54 ± 0.53	0.4752 ± 0.3414	6.154	4.01
B+V	$f_1 = 34.118590(1)$	4.82 ± 0.44	0.4875 ± 0.0918	9.264	1.52
	$f_2 = 6.393003(3)$	1.97 ± 0.44	0.6553 ± 0.2246	8.378	8.11
	$f_3 = 13.645320(4)$	1.42 ± 0.44	0.1436 ± 0.3116	5.979	3.80

Notice: ^{a}The number in brackets are the errors in the last decimal place.